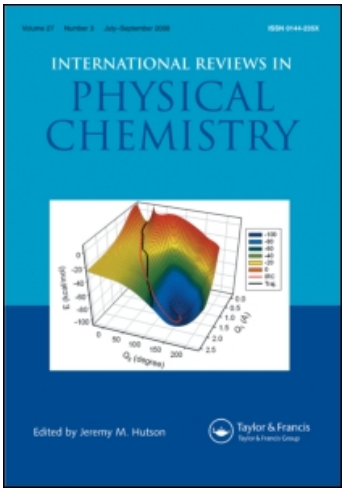

International Reviews in Physical Chemistry
Publication details, including instructions for authors and subscription information:
http://www.informaworld.com/smpp/title~content=t713724383

Surfactant adsorption dynamics

Julian Eastoe; Alex Rankin; Ray Wat; Colin D. Bain

Online publication date: 26 November 2010

To cite this Article Eastoe, Julian , Rankin, Alex , Wat, Ray and Bain, Colin D.(2001) 'Surfactant adsorption dynamics', International Reviews in Physical Chemistry, 20: 3, 357 — 386
To link to this Article: DOI: 10.1080/01442350121251
URL: http://dx.doi.org/10.1080/01442350121251

INT. REVIEWS IN PHYSICAL CHEMISTRY, 2001, VOL. 20, NO. 3, 357–386

Surfactant adsorption dynamics†

JULIAN EASTOE‡, ALEX RANKIN, RAY WAT
School of Chemistry, University of Bristol, Bristol BS8 1TS, UK

and COLIN D. BAIN
Physical and Theoretical Chemistry Laboratory, University of Oxford, South Parks Road, Oxford, OX1 3QZ, UK

Advances in techniques for investigating dynamic adsorption of surfactants at the air–water interface are discussed. Of particular interest are the maximum-bubble-pressure method, and the interrogation of adsorption layers on an overflowing cylinder (OFC) cell using ellipsometry, surface-light scattering, laser Doppler velocimetry and neutron reflection. Recent studies described here, with a model di-chain anionic fluorocarbon surfactant sodium bis(1*H*,1*H*-nonafluoro-n-pentyl) sulphosuccinate (di-CF4) demonstrate that the OFC presents an ideal flexible platform for investigating dynamics of adsorption from solutions. Under certain conditions the behaviour is consistent with an activated-diffusion mechanism, as has been found previously for simple alcohols and various other non-ionic and ionic surfactants.

Contents

† Dedicated to the memory of Professor John C. Earnshaw.

‡ Email: julian.eastoe@bris.ac.uk

International Reviews in Physical Chemistry ISSN 0144–235X print/ISSN 1366–591X online © 2001 Taylor & Francis Ltd
http://www.tandf.co.uk/journals
DOI: 10.1080/01442350110046766

1. Introduction

When a new interface is formed in a surfactant solution, the equilibrium surface tension γ_{eq} is not instantly reached. To reduce γ, surfactant molecules first must diffuse to the surface from the bulk and then adsorb and orient themselves at the interface. Despite decades of work, some important questions concerning the adsorption mechanism remain unanswered. The purpose of this article is to review the current state of knowledge with particular attention to recent results

Figure 1, which is discussed in detail below, depicts various processes involved in adsorption dynamics, which are the focus of this review together with the mechanisms used to describe them. As indicated in figure 2, there is a now an array of experimental techniques that can be used to measure dynamic surface tension $\gamma(t)$, including the maximum-bubble-pressure (MBP), oscillating-jet, inclined-plate, drop-volume, drop-shape and overflowing-cylinder (OFC) methods [1–8].

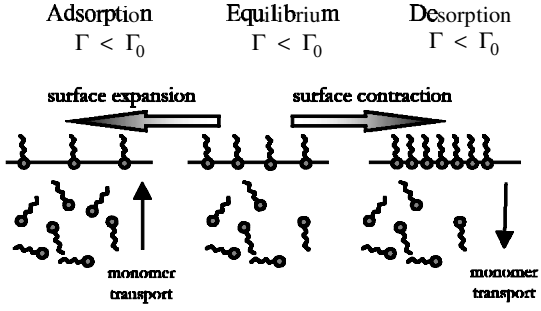

Figure 1. Schematic diagram showing the monomer flux driven by surface expansion and contraction.

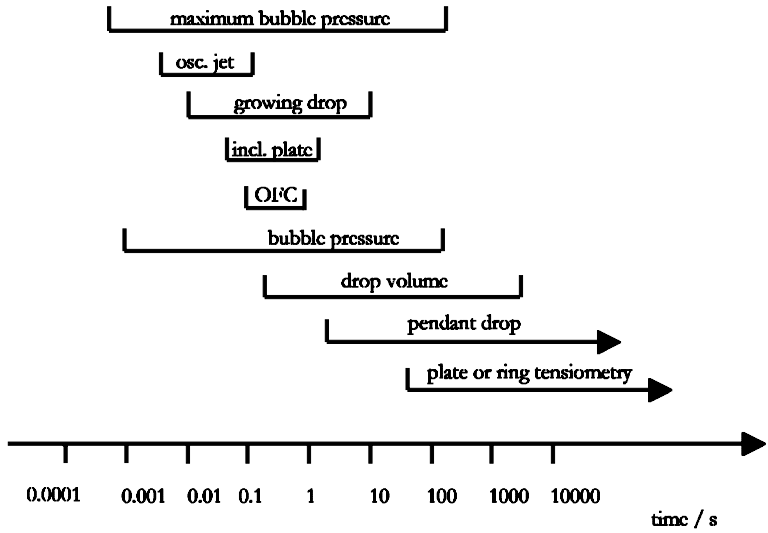

Figure 2. Characteristic time windows for various DST techniques.

By invoking an appropriate isotherm it is possible to infer a rate of surfactant adsorption $\Gamma(t)$. However, a more appropriate method is to measure $\Gamma(t)$ directly by neutron reflection (NR) [9–11].

Dynamic surface tension (DST) is a key property, important in many industrial and biological processes [1, 2]. In the petrochemical industry the DST of aqueous foams assists the efficiency of enhanced oil recovery processes. A well-known example, the manufacture of photographic film and paper, utilizes slide coating of multiple layers of thin gelatin films with high coating speeds and high flow velocity. This requires careful control of the dynamic surface tension in each of the layers to prevent film dewetting and air entrainment. The layers also have to be stable during the drying process, which occurs over a longer time scale, and careful selection of surfactants with appropriate dynamic properties is required.

DST is also essential in agricultural sprays, such as pesticides, which need to be dispersed into a fine spray and then to spread rapidly over leafy surfaces. The stabilization of alveoli by lung surfactant is perhaps the best-known biological application of DST, without which gas transport across the pulmonary membrane would be impossible. DST is, obviously, important in many other wetting, foaming and emulsification processes. In fact, wherever surfactants are employed in processes where the time frame is similar to, or shorter than, that for equilibrium adsorption, the DST will be of interest.

When addressing the problem of dynamic surface adsorption and tension, one should first consider the surface-active species in the bulk. In the simplest case, only monomeric surfactant is present, with the associated bulk diffusion, adsorption and desorption. This can be complicated by the presence of bulk or surface hydrolysis or, when considering proteins, unfolding or denaturation. Sparingly soluble or insoluble surfactants and lipids display irreversible or near irreversible adsorption; so, for simplicity, together with proteins they will not be examined here.

Aggregation is the next issue to consider. Although it is normally assumed that micelles are not surface active, this is not to say that aggregates do not form in the

adsorbed layer, but rather micelles from the bulk solution do not adsorb. Micelles associate and dissociate quickly with time scales between 1 ms and several seconds [12, 13]. Monomer dissociation and adsorption occurs on shorter time scales and complete micellar breakdown and formation on longer time scales. In micellar solutions, the mass transport of monomers is closely linked to that of the micelles and, by inference, monomer convection, diffusion, adsorption and desorption is coupled to the presence and transport of micelles. Therefore, a micelle can best be considered as an active reservoir of surfactant molecules, both as a source of and as a sink for monomer. Although there are reports on dynamic tensions and adsorption of micellar solutions, these systems are not as well understood as for the monomer-only case [14].

There are other possible aggregation structures, including equilibrium and non-equilibrium vesicles, dispersed liquid crystals and solid microcrystallites. Like micelles, these particles are also important as a supply and store of molecules and influence significantly the dynamics of soap lather, the action of lung surfactants [15] and many other practical applications.

Obviously, aggregation introduces experimental and theoretical complexities, some of which are addressed below. The main focus of this review is monomeric (pre-critical micelle concentration (CMC)) solutions, for which good progress has been made recently towards an understanding the underlying adsorption mechanism.

Below follows a summary of relevant theory. In section 3, the surfactants are described. Evidence for an adsorption barrier is reviewed in section 4, and section 5 considers some effects of micelles. In section 6, studies using an OFC are discussed before, in section 7, recent results for a fluorocarbon surfactant are presented. In section 8 results from 11 different non-ionic, anionic and catanionic surfactants are compared, so as to draw some general conclusions.

2. Background theory

2.1. *Adsorption at equilibrium*

At equilibrium the adsorbing flux j_{ads} of monomers to the surface is equal to the desorbing flux j_{des} and this results in an equilibrium surface excess Γ_{eq}. By a combination of tensiometry and NR, it has recently been verified that the equilibrium adsorbed amount can be accessed using the Gibbs equation

$$\Gamma_{eq} = -\frac{1}{nRT}\frac{d\gamma}{d(\ln a)}, \tag{1}$$

where $n = 1$ for non-ionic and zwitterionic surfactants [16–21] and $n = 2$ for 1:1 ionic surfactants (see for example [10, 22]). R is the gas constant, T the temperature and a the activity, which in the case of ionics can be calculated using the Debye–Hückel equation. A variety of tensiometric methods may be employed, such as the du Nouy ring, Wilhelmy plate or drop-volume techniques. Although other isotherm equations are often employed (e.g. those due to Langmuir and to Frumkin), these introduce other effective parameters which are generally unnecessary for analysing DST curves. Therefore, the Gibbs isotherm is entirely adequate for assessing equilibrium adsorption, which (as seen below) is needed as input for modelling DST.

2.2. *Equations for dynamic tension*

In an expanding surface, for example a growing liquid drop or bubble, the surface excess Γ will be less generally than Γ_{eq}, tending to this limiting value at high effective surface ages. Hence, there will be a net flow of surfactant from bulk to interface and hence $j_{ads} > j_{des}$. In the converse case of a contracting surface, Γ is greater than Γ_{eq} and there is a net flow of surfactant from surface to bulk. This can be described simply as

$$\frac{d\Gamma}{dt} = j_{ads} - j_{des}. \tag{2}$$

When a fresh surface is created, there is a flux of monomer from bulk to interface. This flux will cause the surface tension to decay from the solvent tension γ_0 to γ_{eq}, where the surface excess concentration has reached Γ_{eq}. There are two main models for monomer transport and adsorption: diffusion controlled and a mixed kinetic–diffusion model, which are discussed below.

Both models first define a subsurface as an imaginary plane, a few molecular diameters below the interface. The simplest approach is pure diffusion control, which assumes that the monomer diffuses from the bulk into the subsurface, and once in the subsurface it directly adsorbs at the interface. The diffusion process from the bulk to subsurface is the rate-determining step, and the time scale of adsorption from the subsurface to the interface is very fast (of the order of nanoseconds). On the other hand, a mixed kinetic–diffusion model assumes that the rate-determining step is the transport of monomer from the subsurface to the interface, and an adsorption barrier hinders adsorption. This barrier may be due to increased surface pressure or attributed to a lower availability of free surface sites. There may also be steric and orientational constraints on the molecule close to the interface that could prevent adsorption. Thus rather than adsorbing, the molecule will back diffuse into the bulk, thereby lengthening the time required to achieve equilibrium.

2.2.1. *Diffusion control*

The Ward–Tordai equation accounts for diffusion of monomers from bulk to interface, and back diffusion. At the start of the process, monomers from the subsurface adsorb directly, the assumption being that every molecule arriving at the interface is likely to arrive at an empty site. However, as the surface density increases, there is an increased probability that a monomer will arrive at an already occupied site; back diffusion must then also be considered. If the subsurface concentration is known, then the diffusion of molecules from the subsurface to the bulk can also be treated with the Fick equations. The classic Ward–Tordai equation is usually quoted as

$$\Gamma(t) = 2c_0\left(\frac{Dt}{\pi}\right)^{1/2} - 2\left(\frac{D}{\pi}\right)^{1/2}\int_0^{t^{1/2}} c_s d(t-\tau)^{1/2}, \tag{3}$$

where c_0 is the bulk surfactant concentration, D the monomer diffusion coefficient, c_s the concentration in the subsurface, and τ a dummy variable of integration. Owing to the convolution integral, this equation cannot be solved analytically. Asymptotic solutions were proposed by Hansen [23, 24] and Sutherland [25], although these can only be used under certain conditions, such as the dilute limit. It was not until recently that Fainerman *et al.* [26] derived limiting solutions that could easily be applied to DST decays.

2.2.1.1. *Short-time approximation, $t \to 0$.* At the start of the adsorption, there will be no back diffusion and neglecting this term from equation (3) gives

$$\Gamma(t) = 2c_0\left(\frac{Dt}{\pi}\right)^{1/2}. \tag{4}$$

When $\gamma \to \gamma_0$, the surfactant solution can be treated as dilute, and so the linear Henry isotherm can be used to relate Γ and γ:

$$\gamma - \gamma_0 = -nRT\Gamma, \tag{5}$$

where $n = 1, 2$ as above for equation (1). Substituting equation (5) into equation (4) gives the short-time approximation as

$$\gamma_{t\to 0} = \gamma_0 - 2nRTc_0\left(\frac{Dt}{\pi}\right)^{1/2}. \tag{6}$$

2.2.1.2. *Long-time approximation, $t \to \infty$.* As $t \to \infty$, the subsurface concentration approaches the bulk concentration. This allows c_s to be factored outside the back diffusion integral in equation (3), which now tends to unity as $t \to \infty$. Hence

$$\Delta c_{t\to\infty} = c_0 - c_s = \Gamma\left(\frac{\pi}{4Dt}\right)^{1/2}. \tag{7}$$

Considering the Gibbs equation and rearranging gives

$$\gamma_{t\to\infty} = \gamma_{eq} + \frac{nRT\Gamma_{eq}^2}{c}\left(\frac{\pi}{4Dt}\right)^{1/2}. \tag{8}$$

Both equation (6) and equation (8) consider the adsorption as a diffusion-only process, as they are based on the Ward–Tordai equation. Below, in sections 4–8 these equations will be used to probe adsorption mechanisms.

2.2.2. *Mixed diffusion–kinetic control: the presence of an adsorption barrier*

In an activated-diffusion mechanism, monomers undergo diffusion from the bulk to the subsurface, obeying the same diffusion equations as for the diffusion-only mechanism. However, once in the subsurface the monomer is not instantaneously adsorbed. To adsorb successfully it may have to satisfy a number of conditions, for example overcome any potential energy barrier, have the correct orientation for adsorption or strike an 'empty site' in the interface. In addition, the time scale for micelle break-up may hinder adsorption (see below). The term 'adsorption barrier' can be used, as a catchall to incorporate any of or all the above factors that affect surfactant adsorption, that is this would encompass any and all processes, which give rise to deviations from pure diffusion control. This barrier will decrease the adsorption rate, however, if during adsorption none of the above needs to be taken into account, then the process should be purely diffusion controlled, as described in the previous section.

In 1968, Baret [27] described the adsorption process as follows: 'The number of solute molecules that adsorb at the interface is equal to the number of solute molecules which, having diffused from the bulk to the subsurface, cross the adsorption barrier'. It was concluded that the diffusion process is predominant at the start, but there is a switch-over to mixed kinetics as maximum adsorption is attained.

Liggieri and co-workers [28, 29] introduced a renormalized diffusion coefficient, which takes into account both the diffusion to the subsurface and then crossing a barrier to the interface. By employing two activation energies ε_a, a prerequisite for molecules to adsorb, and similarly ε_d for desorption, an Arrhenius-type relationship between D^* (also termed here an effective diffusion coefficient D_{eff}) and D can be introduced:

$$D^* = D\exp\left(-\frac{\varepsilon_a}{RT}\right). \tag{9}$$

Obviously, the mechanism becomes diffusion controlled when $\varepsilon_a \to 0$. The process can be considered as a diffusion problem, which can be solved using the Fick equation, with the new boundary condition

$$\frac{d\Gamma}{dt} = D^*\left(\frac{\delta c}{\delta x}\right)_{x=0}, \tag{10}$$

giving a variation on the Ward–Tordai equation to account for a potential adsorption barrier

$$\Gamma(t) = 2c_0\left(\frac{D_a t}{\pi}\right)^{1/2} - 2\left(\frac{D_a}{\pi}\right)^{1/2}\int_0^{t^{1/2}} c_s d(t-\tau)^{1/2}, \tag{11}$$

where they define

$$D_a = \frac{D^{*2}}{D} = D\exp\left(-\frac{2\varepsilon_a}{RT}\right). \tag{12}$$

This approach to interfacial barriers is described further in [28, 29], and consideration of molecular orientation at the interface in [30–32].

3. Surfactants and tensiometric methods

Pure high quality surfactants are essential if meaningful results are to be obtained in DST studies. This is also important since data derived from equilibrium tensions are needed for interpretation of DST in terms of limiting laws such as equations (1), (6) and (8). This review considers a wide range of surfactants, which are listed in figure 3. Where appropriate, syntheses and purification procedures are described in detail [18, 22, 33–38].

In terms of non-ionics a model di-chained non-ionic glucamide (di-(C6-Glu)) as well as standard alkyl ethoxylates of the form C_iE_j have been studied. With zwitterionics a group of saturated chain symmetric diacyl phosphatidylcholines (di-C*n*)-PC surfactants have been investigated.

Recent studies of an anionic fluorinated compound, sodium bis(1*H*,1*H*-nonafluoro-n-pentyl) sulphosuccinate (di-CF4) are also introduced here. This is an analogue of Aerosol OT (AOT) (sodium bis(2′-ethyl-1-hexyl) sulphosuccinate). The catanionic *n*-hexylammonium dodecylsulphate has also been investigated [33].

The exact form of the adsorption isotherm for 1:1 ionic surfactants is a fundamental issue in surfactant science that is still a matter for some debate. An accurate measurement of the surface coverage is important for explaining many surfactant-related phenomena, especially DST, in which an accurate measure of the adsorption mechanism is essential. The adsorption isotherm can be obtained indirectly by analysing tensiometric data with the Gibbs equation (1). The pre-factor

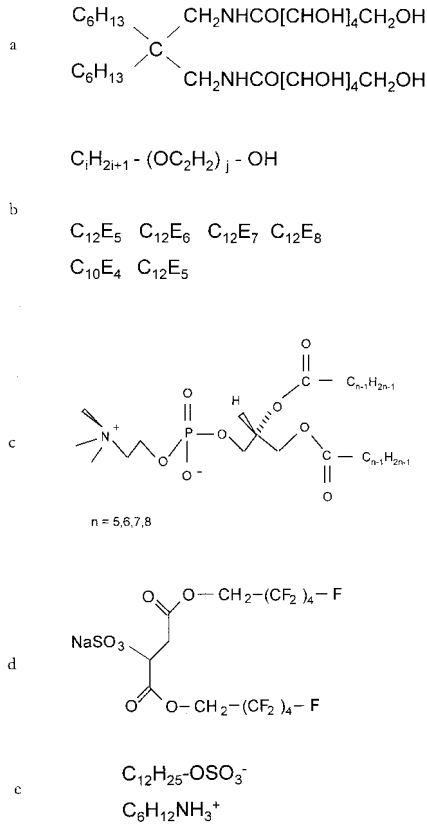

Figure 3. Surfactants used in DST studies. (*a*) the di-chained glucamide (bis[1,2,3,4,5-pentahydroxy hexamindo methyl] n-tridecane or di-(C6-Glu)); (*b*) alkyl ethoxylates C_iE_j; (*c*) zwitterionic diacyl phosphatidylcholines (di-Cn)-PC; (*d*) sodium bis(1*H*,1*H*-nonafluoro-n-pentyl) sulphosuccinate (di-CF4); (*e*) catanionic *n*-hexylammonium dodecylsulphate.

n is dependent on the surfactant type and structure, as well as the presence of extra electrolyte in the aqueous phase. For various zwitterionic and non-ionic surfactants, the expected value of $n = 1$ has been confirmed (see for example [10, 18, 20, 21]). With a 1:1 ionic surfactant, in the absence of extra electrolyte, the thermodynamic treatment requires $n = 2$, implying an equimolar ratio of the surfactant anion and its countercation in the interface [22].

For anionics, the most important contaminants are polyvalent metal ions M^{n+} and the effects have been described in studies of AOT and in several other anionics [22, 38–42]. Even at parts-per-million levels M^{n+} ions can give rise to significant lowering of surface tension in the pre-CMC range [22, 42]. When used at the correct level, the tetrasodium salt of ethylenediaminetetraacetic acid (Na_4 EDTA) is an effective chelating agent, which effectively replaces M^{n+} with Na^+ [22]. Organic impurities can be removed by separation procedures based on foam fractionation [22, 43].

There are various techniques available to measure DSTs, and these have been reviewed and evaluated elsewhere [1, 44, 45]. In this work two main methods are used: drop-volume tensiometry (DVT) and the MBP method. DVT determines the

weight of a drop suspended from a capillary and relies on a balance between surface tension and gravity:

$$V_0 \Delta\rho g = mg = 2\pi r\gamma F, \tag{13}$$

where V_0 is the drop volume, $\Delta\rho$ is the density difference between the two phases, g is the acceleration due to gravity, r is the tip radius, γ is the surface tension and F is a correction factor. Correction factors were obtained by Padday [46] and Harkins and Brown [47], and they depend on $r/V_0^{1/3}$ or r/a, where a is the capillary constant. To measure DST, a modification was introduced by Tornberg [48], which gives rise to time scales ranging from 0.04 s to minutes.

MBP tensiometry has been used extensively to study DST of various surfactant systems (see for example [2, 44, 49–51]). The basis of this technique is measurement of a maximum pressure necessary to blow a bubble in a liquid from the tip of a well-defined capillary. The pressure is increased within the capillary until a bubble appears at the capillary tip, which is immersed in a liquid to a known depth. The pressure in the capillary is maintained constant and an effective surface age is given by the interval between successive bubbles, after corrections for dead time and capillary characteristics [51]. By varying the capillary pressure, this method allows measurement of $\gamma(t)$ for time scales from 1 ms to several seconds.

4. Evidence for an adsorption barrier

4.1. *Studies as a function of concentration*

The experimental section of this review starts by focusing on DST with monomeric neutral surfactants. Recent studies carried out by Lin and co-workers [6, 52, 53] and Eastoe and co-workers [34, 35, 54] both concluded that at higher surfactant concentrations a mixed mechanism operates.

Studies with solutions of decanol (a primitive surfactant) led Lin *et al.* [55, 56] to the conclusion that cohesive forces between the adsorbed molecules play an important role. When the interface becomes saturated, these long-chain alcohols are subject to strong attractive van der Waals forces, which contribute to the observed energy barrier. A Langmuir isotherm was used to account quantitatively for the adsorption rate and to incorporate an activation barrier. The rate of adsorption is, therefore, proportional to a subsurface concentration c_s and the fraction $1 - \Gamma/\Gamma_{max}$ of interfacial sites available for adsorption. The desorption rate is proportional to the surface coverage Γ. The overall rate of adsorption may be written

$$\frac{d\Gamma}{dt} = \left[\beta \exp\left(-\frac{E_a}{RT}\right)\right] c_s(\Gamma_\infty - \Gamma) - \left[\alpha \exp\left(-\frac{E_d}{RT}\right)\right]\Gamma, \tag{14}$$

where β and α are pre-exponential factors for adsorption and description respectively and $E_a(\Gamma)$ and $E_d(\Gamma)$ are activation energies for adsorption and desorption respectively. The adsorption rate constant is defined as $\beta \exp(-E_a^0/RT)$ and Γ_∞ is the maximum number of available sites.

To account for the increase in activation energy with increasing surface pressure, the activation energies are a function of Γ:

$$E_a = E_a^0 + \nu_a \Gamma^n, \tag{15}$$

$$E_d = E_d^0 + \nu_d \Gamma^n, \tag{16}$$

where E_a^0, E_d^0, ν_a and ν_d are all constants.

At equilibrium, $d\Gamma/dt = 0$, and the equilibrium isotherm becomes

$$\frac{\Gamma}{\Gamma_\infty} = x = \frac{c}{c + a\exp(kx^n)}, \tag{17}$$

where $k = (\nu_a - \nu_d)\Gamma_{max}^n/RT$ and $a = (\alpha/\beta)\exp[(E_a^0 - E_d^0)/RT]$. When $n = 1$, the Frumkin isotherm results and, when $\nu_a = \nu_d = k = 0$, equation (17) reduces to the Langmuir isotherm. From the reported pendant drop experiments on decanol, it was shown that a switch-over in adsorption mechanism from diffusion control to mixed kinetic–diffusion control occurs on longer time scales. This is consistent with an activation barrier, which develops when the attractive van der Waals forces are sufficiently large at higher interfacial concentrations.

Lin and co-workers [52, 53] have also studied two non-ionic alkyl ethoxylates: $C_{12}E_8$ and $C_{10}E_8$. For both these surfactants, they also concluded that a switch-over in adsorption mechanism, from diffusion to mixed kinetic–diffusion control, could take place as a function of bulk concentration. In figure 4 (*a*), the DST curves for $C_{10}E_8$ solutions are given, for a wide range of pre-CMC concentrations. Figure 4 (*b*) shows how the effective diffusion D_{eff} decreases as the concentration is increased. These results suggest adsorption of $C_{10}E_8$ molecules on to a clean air–water interface is not purely diffusion controlled. It should be pointed out that these values were obtained by applying different adsorption isotherms, and further information can be found elsewhere [52, 53, 55, 56]. They also observed that by using the Frumkin isotherm, rather than the Langmuir isotherm, they were able to achieve greater agreement with measured data, from which one can infer that intermolecular interactions between adsorbed molecules are significant.

4.2. *Effect of temperature*

As has already been mentioned, the type and quality of surfactant are important factors since impurities may contribute to any observed adsorption barrier. It is also essential to have a firm grasp of the adsorption dynamics of simple non-ionics, before investigating the more complicated ionic systems. Certain non-ionics are ideal as their equilibrium adsorption properties are well documented. The di-(C6-Glu) surfactant (see figure 3) is one such surfactant and was, therefore, chosen for a detailed dynamic study [57–60]. Di-(C6-Glu) is particularly well suited to this as there is no cloud point below 90°C. In addition, extensive du Nouy measurements over the range 10–50°C show that both the CMC and the maximum adsorbed amount Γ_{max} are essentially constant; they may be taken as $(1.35 \pm 0.05) \times 10^{-3}$ mol dm^{-3} and $(2.75 \pm 0.25) \times 10^{-6}$ mol m^{-2} respectively [58–60]. Pulsed field gradient spin echo (PFGSE) nuclear magnetic resonance (NMR) was used to measure the monomer self-diffusion coefficient D below the CMC at 8.0×10^{-4} mol dm^{-3} and a temperature of 25°C [35, 61], and this gave $D = 2.70 \times 10^{-10}$ m^2 s^{-1}.

The DSTs were measured as a function of temperature in order to be assessed by the Arrhenius-type expression suggested by Liggieri and co-workers (equation (9)). Although it is generally accepted that the initial adsorption, where the surface coverage is low, is purely diffusion controlled, there is still some controversy about the underlying mechanism closer to equilibrium. These experiments show that for this monomeric non-ionic surfactant, the final stages of the $\gamma(t)$ decay as a function of temperature are consistent with Arrhenius-like behaviour, and an activated-diffusion controlled adsorption mechanism.

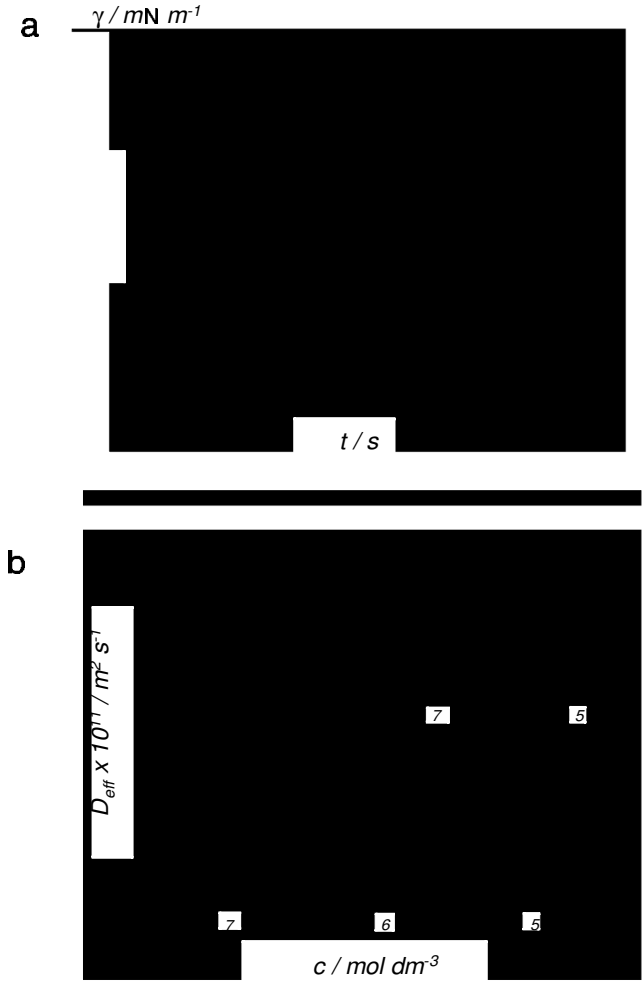

Figure 4. (*a*) DSTs for $C_{10}E_8$ solutions according to Lin and co-workers [52, 53] for various concentrations: curve 1, 0.20×10^6 mol dm^{-3}; curve 2, 0.50×10^6 mol dm^{-3}; curve 3, 1.0×10^6 mol dm^{-3}; curve 4, 2.0×10^6 mol dm^{-3}; curve 5, 4.0×10^6 mol dm^{-3}; curve 6, 6.0×10^6 mol dm^{-3}; curve 7, 10.0×10^6 mol dm^{-3}; curve 8, 30.0×10^6 mol dm^{-3}. (*b*) Effective diffusion coefficients D_{eff} derived from DST data. (Reproduced with permission from the American Chemical Society.)

For non-ionics, equation (8) is

$$\gamma(t)_{t\to\infty} = \gamma_{\text{eq}} + \frac{RT\Gamma^2}{2c}\left(\frac{\pi}{Dt}\right)^{1/2}, \tag{18}$$

where γ_{eq}, c, Γ and D represent the equilibrium tension, bulk concentration, surface excess and monomer diffusion coefficient respectively of the surfactant (see section 2.2.1.2). If the adsorption were purely diffusion controlled, then this equation should account reasonably well for the end of the tension decays (a rigorous analysis of this equation indicates that this approach is valid for investigating the adsorption mechanism [2, 62]).

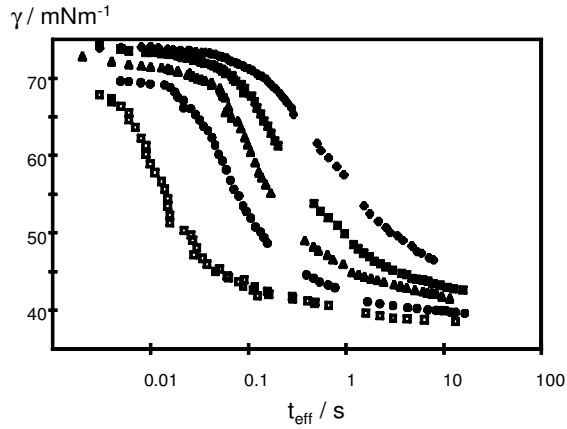

Figure 5. DSTs for solutions of di-(C6-Glu), below the CMC at 5×10^{-4} mol dm^{-3}, as a function of temperature T: (◇), 10°C; (■), 20°C; (△), 30°C; (●), 40°C; (□), 50°C. (Reproduced with permission from the American Chemical Society.)

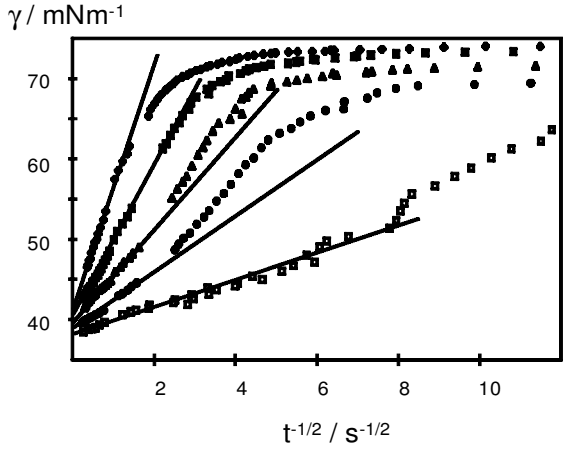

Figure 6. DST data of figure 5 plotted against $t^{-1/2}$ in line with equation (18): (——), least-squares fits with $\gamma = \gamma_{eq}$ as $t \rightarrow \infty$. (Reproduced with permission from the American Chemical Society.)

Figure 5 shows the DST of di-(C6-Glu) as a function of temperature measured by the MBP method, and it is clear that increasing T gives rise to a faster decay. The equilibrium surface tension was measured as a function of T by du Nouy tensiometry, with γ_{eq} decreasing from 41.0 mN m^{-1} at 10°C to 36.9 mN m^{-1} at 50°C. Between 20 and 50°C the DST decays were therefore essentially complete, with the final points close to the du Nouy values. At 20°C the last DST measurement was 1.8 mN m^{-1} above γ_{eq} and at 50°C this difference was 0.7 mN m^{-1}. The difference in γ_0 (the surface tension of the solvent) at the start of the decay is consistent with the effect of temperature for water.

In order to test equation (18) the DST data are plotted as a function of $t^{-1/2}$ in figure 6. The data linearize at long times, suggesting a diffusion-type process. The lines are least squares fits for $t > 0.25$ s (i. e. $t^{-1/2} < 2$), with the intercepts equal to

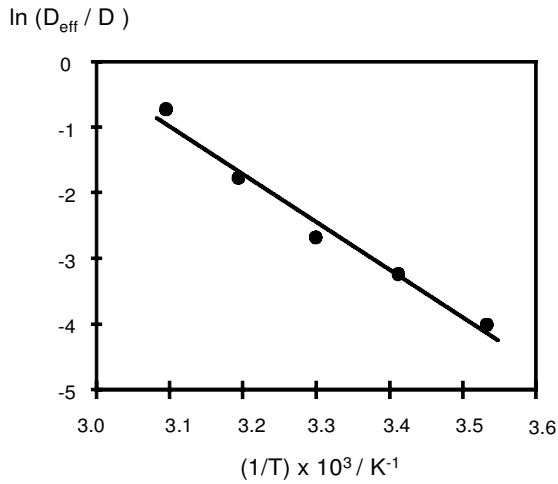

Figure 7. Arrhenius-type plot for a di-(C6-Glu) solution at 5×10^{-4} mol dm^{-3}: (——), fitted line giving $\Delta H = +62$ kJ mol^{-1}. (Reproduced with permission from Elsevier.)

the equilibrium tensions measured by the du Nouy ring. The gradients of these fitted lines were used to estimate effective diffusion coefficients using

$$D_{\text{eff}} = \left(\frac{RT\Gamma^2 \pi^{1/2}}{2c \times \text{gradient}} \right)^2, \tag{19}$$

which can be obtained by rearranging equation (18). The monomer self-diffusion coefficient D (equal to 2.70×10^{-10} m^2 s^{-1} at 25°C), obtained from PFGSE NMR measurements was used to estimate D values at the other temperatures [35]. Both the temperature T and the viscosity η of the solution will have an effect on D, and each of these will be considered in turn. Firstly, giving attention to temperature, assuming that a Stokes–Einstein-like relationship holds for the solutions studied here, then $D \propto T$. Viscosity has a larger effect on D, as its relationship is exponential with temperature.

Combining these two effects gave D values at each temperature. Figure 7 is an Arrhenius plot in line with equation (12). Note that changes in D over this temperature range are small compared with the increase in D_{eff}. For example at 10°C the value of D is 36% of that at 50°C, whereas for D_{eff} this value is 1.4%. At 10°C the ratio D_{eff}/D is 0.018, indicating that the measured tension is substantially higher than that predicted by equation (18) and that there is a significant adsorption barrier. At 50°C the ratio D_{eff}/D is relatively close to 1, suggesting a nearly diffusion-controlled adsorption at this temperature.

Alternatively, the Hansen [23, 24] equation

$$\gamma(t)_{t \to \infty} = \gamma_{\text{eq}} + \frac{RT\Gamma^2}{c} \left(\frac{1}{\pi D t} \right)^{1/2} \tag{20}$$

could also be used and this results in a D_{eff} value aproximately 2.5 times lower than equation (19).

Calculations by Liggieri and co-workers [28, 29] showed that E_a can cause a significant decrease in the adsorption $\Gamma(t)$, especially in the long-time limit. Relatively small barriers can have a significant effect and, for any given time, raising

E_a will increase γ. For example at 10 s, with a surfactant molecular weight of 600, the predicted adsorptions for E_a equal to $1.1RT$ and $3.2RT$ are a factor of five and a factor of ten respectively lower than those for a purely diffusion-controlled adsorption. However, at short times, $\gamma(t)$ data cannot be used to discriminate clearly between diffusion-only and mixed mechanisms. A number of alternative theoretical approaches have also been proposed [62–67] and, although these treatments have met with some success, they do not appear to be applicable to the results presented here.

The activation barrier may also be expressed simply as

$$D_{\text{eff}} = D \exp\left(-\frac{\Delta G}{RT}\right), \tag{21}$$

where ΔG represents the free energy change for the formation of an activated state. The separate entropy contribution ΔS and enthalpy contribution ΔH can be introduced and then

$$D_{\text{eff}} = D \exp\left(\frac{\Delta S}{R}\right) \exp\left(-\frac{\Delta H}{RT}\right) \tag{22}$$

or

$$\ln\left(\frac{D_{\text{eff}}}{D}\right) = \frac{\Delta S}{R} - \frac{\Delta H}{RT}. \tag{23}$$

Of course it must be assumed that the activation parameters do not depend significantly on temperature, at least over the range studied. For the di-(C6-Glu) the data in figure 7 yield an apparent enthalpy change $\Delta H = +62 \pm 1\,\text{kJ mol}^{-1}$ and an apparent entropy change $\Delta S = +180 \pm 5\,\text{J K}^{-1}\,\text{mol}^{-1}$.

In figure 8 values for $-\ln(D_{\text{eff}}/D)$ are shown as a function of concentration, at 25°C, for various non-ionic surfactants (see key), above and below their CMCs which are marked. Broadly speaking, the ratio D_{eff}/D appears to be independent of both surfactant type and concentration, both below and above the CMC. Using equation (21) the mean value of ΔG is $+7.5\,\text{kJ mol}^{-1}$, and this is consistent with ΔH and ΔS determined in the temperature variation experiments ($62 - 54 = 8\,\text{kJ mol}^{-1}$).

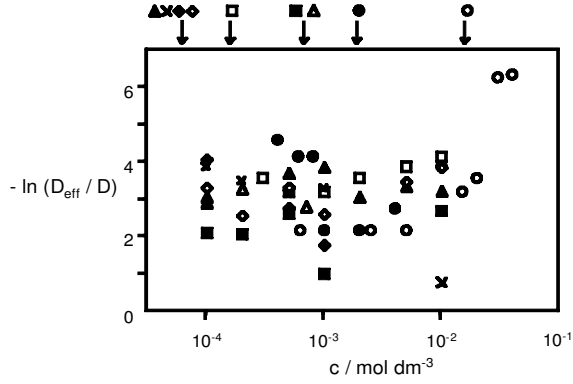

Figure 8. Values of $-\ln(D_{\text{eff}}/D)$ versus concentration c for various C_nE_m and glucamide surfactants, where the arrows indicate the CMCs: (■), $C_{10}E_4$; (△), $C_{10}E_5$; (▲), $C_{12}E_5$; (◇), $C_{12}E_6$; (◆), $C_{12}E_7$; (×), $C_{12}E_8$; (○), di-(C5-Glu); (●), di-(C6-Glu); (□), di-(C7-Glu). (Reproduced with permission from Academic Press.)

The values for the thermodynamic parameters suggest both temperature and concentration variation experiments can be reconciled by formation of an activated state. Some insight into the nature of this pre-adsorbed state may be gained by comparing the activation parameters with ΔH_{ads} and ΔS_{ads} values for adsorption at equilibrium [68]. With C_{12} ethoxylated sulphonates and sulphates Rosen and Song [68] found ΔH_{ads} ranging from +2.4 to −12.5 kJ mol^{-1}, with ΔS_{ads} between about 80 and 110 J K^{-1} mol^{-1}. (Although they are anionic, these surfactants do also contain EO groups, like the non-ionics discussed here.) The entropy changes are consistent with the hydrophobic effect, and a 'release of ordered water molecules'. The formation of the activated state is endothermic whereas, for the equilibrium state, ΔH_{ads} is generally exothermic. These differences may reflect an energy requirement for molecules to attain sufficient energy to penetrate the film.

Miller *et al.* [2] have also seen similar DST behaviour with temperature. For a pre-CMC solution of Triton X-100 at 1.55×10^{-4} mol dm^{-3} it was observed that $d\gamma/dt^{-1/2}$ also decreases with increasing temperature. For example at 30°C the slope was 17 mN m^{-1} s$^{1/2}$ whereas at 70°C it was 8 mN m^{-1} s$^{1/2}$. Using estimated values for $D \approx 2.6 \times 10^{10}$ m^2 s^{-1} and $\Gamma = 2.65 \times 10^{-6}$ mol m^{-2} this is consistent with an enthalpy of activation of about 40 kJ mol^{-1} for this technical-grade surfactant.

5. Dynamic surface tension with micellar non-ionic surfactant solutions

It has been proposed that the presence of micelles may also play a role in DST. If the overall micellar lifetime τ_2 [69–71] is longer than the time taken for $\gamma(t)$ to reach γ_{eq}, then the micellized surfactant may not be available for adsorption, and hence the DST will decay more slowly. Adsorption of monomers results in a concentration gradient in the subsurface, which would be reduced by the usual diffusion of monomers in the bulk and also by the break-up of micelles in the subsurface region. It is reasonable that the aggregation number, which is linked to τ_2, may influence the adsorption dynamics. Rillaerts and Joos [72] and later Fainerman [73] and Fainerman and Makievski [74–76] turned this argument around to obtain estimates for rate constants k_{mic} ($\propto 1/\tau_2$) from DST measurements on micellar solutions. This study [72] yielded the following relationship between k_{mic} and $\gamma(t)$:

$$\gamma(t)_{t\to\infty} = \gamma_{eq} + \frac{nRT\Gamma^2}{2c_0 t}\left(\frac{\pi}{Dk_{mic}}\right)^{1/2}. \tag{24}$$

Fainerman and Makievski suggested that equation (24) should be used rather than equation (20) above the CMC. In order to test this approach, k_{mic} values were measured for some C_nE_m surfactants using the absorbance stopped-flow method [37]. For certain compounds the values of k_{mic} were in good agreement with similar measurements by Tiberg *et al.* [77]. Both methods gave k_{mic} for $C_{12}E_5$ and $C_{12}E_6$ as 0.10 and 0.17 s^{-1} respectively. Using $C_{12}E_5$ as an example, DST decays suggested by equation (24) were synthesized using the measured values of k_{mic}, D and Γ, as shown on figure 9.

The predicted tension is too low at low micellar concentrations, and too high at higher concentrations. It would appear that micelle dissociation might be important when the monomer subsurface concentration is limiting, or k_{mic} is small. These conditions occur with very hydrophobic surfactants where the CMCs are low, and also having long micellar lifetimes (stable micelles). It was seen that, even for the most hydrophobic surfactant studied, namely $C_{12}E_5$, where the CMC is

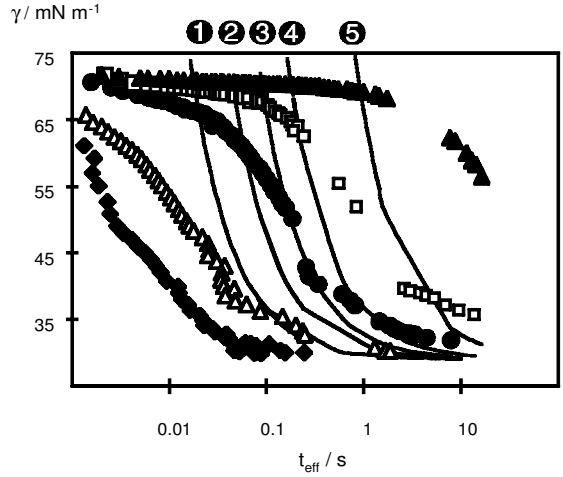

Figure 9. DSTs of $C_{12}E_5$ micellar solutions (◆, △, ●, □, ▲) and calculations (❶, ❷, ❸, ❹, ❺) accounting for micellar kinetics using the Fainerman–Makievski equation (24) for various concentrations: (◆), (❶), 100 CMC; (△), (❷), 40 CMC; (●), (❸), 20 CMC; (□), (❹), 10 CMC; (▲), (❺), 2 CMC. (Reproduced with permission from Elsevier.)

approximately 5×10^{-5} mol dm^{-3} and $\tau_{mic} \approx 10$ s, the DST decays were best described by incorporating an activation barrier into the Miller diffusion equations (equations (20) and (21)).

One possible explanation has been discussed by Johner and Joanny [78] for A–B block copolymers. They suggested that release of monomer from micelle to the bulk is an important process (τ_1), rather than complete micellar breakdown (τ_2). Hence micelles in the subsurface can 'leak', releasing one or two molecules. Since τ_1 is typically 10^{-6}–10^{-4} s [69–71], the micelles can be thought of as a source of monomers.

6. Surface light scattering and neutron reflection studies using the overflowing-cylinder technique

This section describes recent developments in experimental methods for making direct measurements of $\gamma(t)$ and $\Gamma(t)$. Several techniques have been developed for measuring $\gamma(t)$, of which the MBP method is perhaps the most widely used. However, the dynamic adsorbed amount $\Gamma(t)$ is the fundamental quantity of interest and is much more difficult to measure directly; it can be inferred from $\gamma(t)$, but only if the assumption that $\Gamma(t)[\gamma] = \Gamma_{eq}[\gamma]$ is correct.

Analysis of MBP data is complicated by the variation in expansion rate during bubble growth and the dependence of the surface on adsorption history. Steady-state techniques such as the jet [49], inclined-plate [49] and OFC [7–9, 79–81] methods present significant advantages over the MBP and other time-dependent techniques. High-pressure jets are suitable for studying dynamics down to the millisecond time scale [4], whereas inclined-plate cells can be used for longer time scales (approximately 1 s). In the latter case flow instabilities have complicated attempts to measure $\Gamma(t)$ by NR.

The OFC employed here is suitable for measurements on the 0.1–1 s time scale. The surface properties of this cell, and in particular the relationship between the

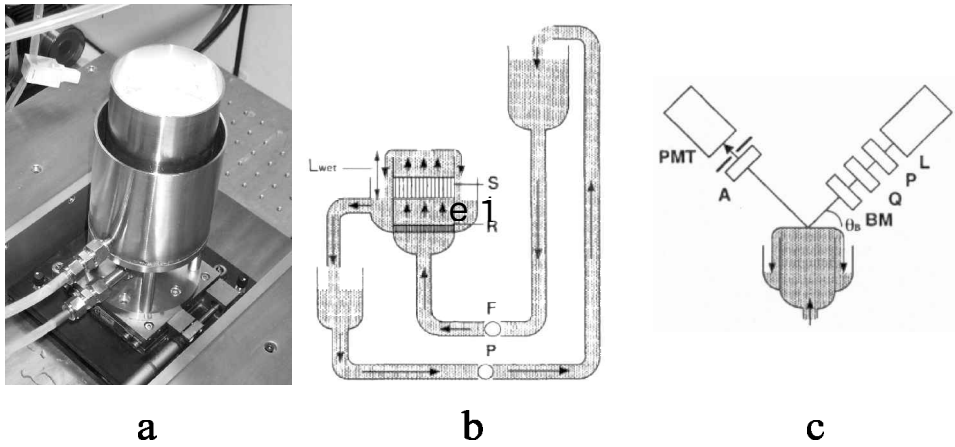

Figure 10. (*a*) Looking down on the OFC cell. (*b*) Schematic diagram of the OFC cell: S, flow straightener; R, resistance plate; F, flowmeter; P, magnetic drive pump; L_{wet}, wetting length. (*c*) Schematic diagram of the OFC on the Beaglehole ellipsometer: L, He–Ne laser; P, polarizer; Q, quarter-wave plate; BM, birefringence modulator; θ_B, Brewster angle; A, analyser; PMT, photomultiplier tube. ((*b*) and (*c*) are from [7]; reproduced with permission from Academic Press.)

surface excess, surface expansion rate and bulk concentration, depend solely on adsorption kinetics at that particular concentration and surface excess. The OFC is particularly attractive as it offers a large (approximately 50 cm^2), almost flat surface for analysis by ellipsometric, spectroscopic and other scattering techniques. Since the surface is at a steady state, experiments lasting up to several hours can be performed to improve the signal-to-noise ratio, for example for NR at low surface coverages. However, as Maringoni effects determine the surface expansion rate, the rate is independent of the bulk flow rate [7]. Consequently, adsorption kinetics can only be studied at a single surface concentration for any given bulk concentration. This surface concentration is determined by the geometry of the OFC. The OFC also requires a bulk solution of approximately 1.5 litres and thus, when working with deuterated materials for NR studies, the amount and cost of surfactant required becomes a consideration. In contrast, with the MBP technique the sample volume is approximately 12 ml, and this can produce data on time scales from milliseconds to seconds, and hence for all surface excesses from near zero to equilibrium coverage. Fortunately the time scale accessible for the OFC method is of considerable interest for practical applications of surfactants.

The OFC (figures 10 (*a*) and (*b*)) consists of a stainless steel cylinder, 80 mm in diameter and 140 mm tall. Liquid is pumped vertically upwards through a baffle that reduces the height required to ensure plug flow. The liquid flows over the top rim of the cylinder, achieving a pure steady state of the horizontal surface. On the outside of the cylinder a wetting film is formed. The surface flows radially from the centre towards the rim. In the presence of a surfactant, the surface tension gradient can increase the surface velocity by an order of magnitude, compared with that for pure water. The surface expansion rate is typically in the range 1–10 s^{-1}, which for dilute surfactant solutions leads to a surface that is far from equilibrium. The surface properties can be characterized by a variety of methods, for example, the surface expansion rate can be determined by laser Doppler velocimetry (LDV), while $\gamma(t)$

can be obtained by ellipsometry and surface light scattering (SLS), as described below.

6.1. *Ellipsometry*

Ellipsometry measures the change in polarization of light reflected from a liquid surface and is dependent on the thickness of the adsorbed layer and its refractive index. The polarization can be related to the surface excess of the surfactant solution. The technique is extremely sensitive to the presence of surfactant on the surface of water and measurements can be made with a precision of less than 1% of a monolayer, in just a few seconds.

A typical set-up used is given in figure 10 (*c*). Polarization of a He–Ne laser is modulated photelastically at 50 kHz by a quartz plate and then directed on to the surface of the liquid in the OFC at the Brewster angle θ_B. Reflected light is detected by a photomultiplier tube and lock-in amplifiers extract the signals at 50 and 100 kHz. The coefficient of ellipticity is recorded every second and an average over 50 readings is calculated [7].

The Brewster angle for a real interface is defined as the angle at which $\mathrm{Re}\,(r_p/r_s) = 0$, where r_p and r_s are reflection coefficients for light polarized in the plane of incidence and light polarized in the plane of the surface respectively. If the thickness of the monolayer is much smaller than the incident wavelength, then the θ_B values for both real and ideal interfacial models are the same, and the coefficient $\bar{\rho}$ of ellipsometry, also known as ellipticity, is given by $\mathrm{Im}\,(r_p/r_s)$ at θ_B [7]. To convert dynamic ellipticity into surface tension, it must be assumed that the adsorbed film is at local equilibrium with the solution immediately below the surface. Calibration curves can then be generated from equilibrium measurements on stationary solutions [7].

Although $\bar{\rho}$ is determined directly by the adsorbed monolayer, it is not in itself an absolute measure of surface concentration Γ. Under certain conditions, there is a linear relationship between $\bar{\rho}$ and Γ [82], but such a relationship cannot be assumed to hold for all surfactants. Generally, ellipsometric data must be calibrated against a direct measurement of surface excess, obtained, say by NR.

6.2. *Laser Doppler velocimetry*

A more thorough description of LDV (or anemometry) has been given by, among others, Drain [83] and Durst *et al.* [84]. In a differential laser set-up, two coherent laser beams are crossed in a probe volume. Particles intercepting the probe volume scatter light from both beams in all directions. A detector viewing the probe volume measures the intensity of scattered light. The light scattered by moving particles is Doppler shifted; however, the shift with respect to the two beams is not the same, causing a fluctuating intensity on the detector. The fluctuation frequency f equals the difference between these Doppler shifts and is given by

$$f = \frac{2v_x \sin(\theta/2)}{\lambda}, \tag{25}$$

where λ is the wavelength of the incoming laser light, θ is the angle between the two intersecting beams and v_x refers to the particle velocity component lying in the beam plane and perpendicular to the beam bisector. Hence, the relation between f and v_x is determined by optical and geometrical parameters only.

Using an OFC, light beams are made to cross exactly in the expanding surface in such a way that the bisector of the beam directions is perpendicular to the expected direction of the surface velocity. Consequently applying equation (25) to the OFC surface, the surface radial velocity v_r may be directly substituted for v_x. When moving the probe volume over an imaginary line radiating from the centre of the meniscus, the distribution of v_r in the surface can be studied. The light beams reflect from the surface in the probe volume, and the Doppler anemometer ensures that only velocity information of the surface will be obtained. Experimental results have proved that the incidence angle α does not influence the Doppler frequency; however, as predicted by equation (25) it is dependent on θ.

Experimentally particles of TiO_2 (2 μm) (Fluka) are suspended in the surfactant solution to act as scattering centres at the interface. The concentration of particles is adjusted to ensure that there would typically be only one particle within the probe volume at any given time. The Fourier transformed output from the photomultiplier tube is averaged over typically 300 scans and the peak frequency converted into surface velocity using equation (25). Plots of surface velocity as a function of radial distance are fitted using

$$v_r(z=0) = a_1\frac{r}{R} + a_3\left(\frac{r}{R}\right)^3, \tag{26}$$

where R is the cylinder radius. Near the cylinder centre, where $r \ll R$, only the leading-order term in v_r is needed. The surface expansion rate $\theta = (1/r)\,\mathrm{d}(rv_r)/\mathrm{d}r$, is then independent of r:

$$\theta = \frac{2a_1}{R}. \tag{27}$$

6.3. *Surface light scattering*

SLS is a modern non-perturbative technique that can determine surface tension with static or flowing liquid surfaces [85]. The surface of a liquid consists of thermally generated capillary waves and, in the presence of an adsorbed monolayer, they may be coupled to dilational waves. SLS may be used to study these waves over the frequency range 10^4–$10^6\ \mathrm{s}^{-1}$. These can be considered as a Fourier series of surface waves of wavelength Λ, each with a well-defined frequency ω, decaying as

$$\omega = \omega_0 + \mathrm{i}\Gamma, \tag{28}$$

where in this case Γ is the damping constant. The wavenumber q is given by

$$q = \frac{2\pi}{\Lambda}. \tag{29}$$

These surface waves may be analysed using a method developed by Earnshaw *et al.* [86] and surface properties can be obtained. When coupled with the OFC method, this becomes a useful non-invasive measurement of $\gamma(t)$ [8]. For a monolayer covered liquid surface, ω and q are related by a dispersion equation

$$D(\omega) = 0, \tag{30}$$

where

$$D(\omega) = \left(\frac{\varepsilon q^2}{\omega} + \mathrm{i}\eta(q+m)\right)\left(\frac{\gamma q^2}{\omega} + \frac{g\rho}{\omega} - \frac{\omega\rho}{q} + \mathrm{i}\eta(q+m)\right) + [\eta(q-m)]^2 \tag{31}$$

and

$$m = \left(\frac{q + i\omega\rho}{\eta}\right)^{1/2}, \quad \mathrm{Re}\,(m) > 0. \tag{32}$$

η and ρ are the bulk viscosity and density respectively.

γ and ε, the transverse and dilational moduli respectively, can be expanded to take into account dissipative effects within the film to give

$$\gamma = \gamma_0 + i\omega\gamma', \quad \varepsilon = \varepsilon_0 + i\omega\varepsilon', \tag{33}$$

where γ_0 is the surface tension and ε_0 the dilational elastic modulus. As for γ' and ε', they can be considered to be surface viscosities, that is the transverse shear and dilational viscosities respectively, and primarily act to increase the damping of the capillary and dilational waves respectively. ε_0 can be written as

$$\varepsilon_0 = -\frac{d\gamma_0}{d \ln \Gamma_s}, \tag{34}$$

where Γ_s is the surface excess.

The data may be analysed by two methods. The first gives unbiased estimates of the frequency ω_0 and damping constant Γ of capillary waves of the experimental q. The second method generates the four surface properties γ_0, γ', ε_0 and ε' directly from the measured correlation function. This involves fitting the data with the Fourier transform of the theoretical spectrum of thermally excited capillary waves on a surface supporting a molecular film, expressed as a function of the above parameters [86, 87].

6.3.1. *Experimental set-up*

The laser beam is first spatially filtered before passing through a 'weak' transmission grating that generates a series of diffracted beams. The lenses image the grating at the liquid surface, and diffracted orders converge at the surface and then diverge to form a series of reference beams at the photomultiplier tube. In order to achieve normal incidence geometry a polarizing beam splitter and a quarter-wave plate are employed.

The set-up has been described in detail elsewhere [88], but a schematic diagram is given in figure 11.

6.4. *Neutron reflection*

Since the adsorbed amount is the fundamental parameter, a direct method for measuring both Γ_{eq} and $\Gamma(t)$ is desirable. Early experiments employed radiotracer measurements using tritiated surfactants [39, 89–91], more recently surface second-harmonic generation spectroscopy [92] and NR (see for example [17, 18, 20, 21, 40, 41, 93]). For NR, the surface excess around the CMC can be measured to about 5% [94], whereas the accuracy of the other two methods is rather more difficult to assess. The absolute amount of surfactant ion in the monolayer (see for example [17, 18, 20, 21, 40, 41, 93]) can be obtained by NR measurements, using null reflecting water (NRW) (8 mol% D_2O). The measured reflectivity curve can be modelled in terms of a single uniform layer to fit for thickness τ and scattering length density ρ. These values are related to A via

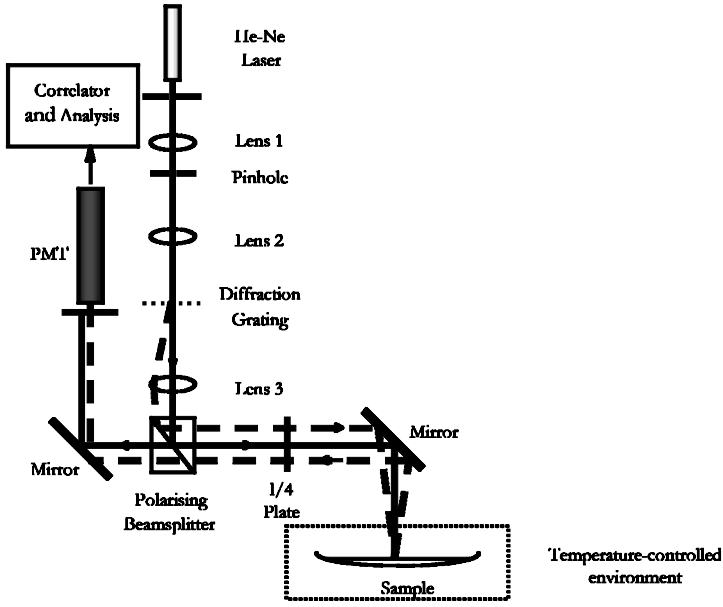

Figure 11. Schematic set-up for SLS. (From [88], reproduced with permission from the American Chemical Society.)

$$A = \frac{\sum_i b_i}{\rho\tau} = \frac{1}{\Gamma N_A}. \tag{35}$$

The sum $\sum_i b_i$ of nuclear scattering lengths over the surfactant molecule can be calculated from known values, and N_A is the Avogadro number. It is worth noting that NR is a direct method, which essentially 'counts' molecules in the film, while tensiometry is indirect, and interpretation of the γ-a curve always involves assumptions in terms of an adsorption equation. This represents the main benefit of having supplementary information from NR for interpreting DST data.

6.4.1. *Experimental set-up*

NR measurements were performed on the CRISP and SURF reflectometers at ISIS, Rutherford Appleton Laboratories, Didcot, UK, using the standard set-up for free liquid surfaces [10, 11, 95, 96]. The dynamic NR OFC experiments were carried out on the SURF beam line and the experimental layout is shown in figure 12 [9].

Two slits S1 and S2 collimate the beam before the incident flux is measured by the monitor M (see caption to figure 12). Using the OFC with pure water only (D_2O needed for calibration [10, 11, 95, 96]) there is an increasing surface curvature near the rim owing to surface tension. (This curvature effect is also evident at the lower end of surfactant concentration but disappears for tensions below about $50\,mN\,m^{-1}$.) Therefore, S2 is used to reduce the beam footprint, eliminating edge effects, and slits 3 and 4 limit background scattering at the final detector.

The specular neutron reflection $R(Q)$ is measured normal to the interface as a function of the momentum transfer $Q = (4\pi \sin\theta)/\lambda$. The incidence angle θ is 1.5°, and incident wavelengths are 0.5–6.5 Å, resulting in an accessible Q range of 0.05–0.65 $Å^{-1}$. Measurements are carried out at selected surfactant concentrations using

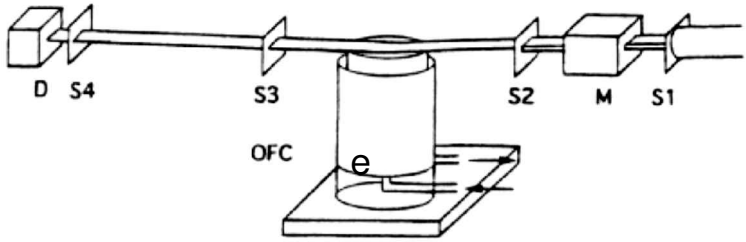

Figure 12. Schematic set-up of the OFC cell with NR: S1, S2, S3, S4, slits; M, incident beam monitor; D, final detector. Neutrons enter from the right, and in fact the monitor is to the left of slit S2. (From [9]; reproduced with permission from the American Chemical Society.)

NRW. The reflectometer is calibrated with D_2O, and a flat background of about 5×10^{-6} (determined by extrapolation of the data to high Q) was subtracted [95, 96]. This approach is generally considered valid when there is no small-angle scattering from the bulk, which is a reasonable assumption at low surfactant concentrations. Full accounts of the theory can be found elsewhere (see for example [10, 11]); however, under these conditions the $R(Q)$ curve can be modelled in terms of a single, uniform layer using the optical matrix method. The $R(Q)$ decays are fitted by a least squares programme [95] to yield the layer thickness τ and scattering length density ρ, and hence the area per molecule or surface excess via equation (35).

7. Adsorption dynamics of a model fluorocarbon surfactant

In order to investigate the dynamic adsorption mechanism measurements on the OFC by SLS, NR and LDV have been made, together with further dynamic measurements by MBP and equilibrium characterization by DVT. The long-time approximation of the Ward–Tordai dynamic adsorption model is given in equation (8) (see section 2.1.2.2). These separate parameters can be measured independently by the above techniques and the free monomer diffusion coefficient can be evaluated by PFGSE NMR ($D = 1.66 \times 10^{-10}\,m^2\,s^{-1}$) (see for example [61]). Therefore, the validity of this approach can be tested.

The di-chain anionic surfactant di-CF4 shown in figure 3 (*d*), has been carefully selected to possess a number of key features [38].

(i) Synthesis has been thoroughly characterized.
(ii) Surface purity has been also been painstakingly characterized.
(iii) DST decay is in the appropriate time frame for the MBP and OFC methods.
(iv) Being a fluorocarbon, the refractive index for light, and also neutrons, results in a good signal-to-noise ratio in surface scattering experiments.
(v) Since with fluorocarbons there is a low equilibrium tension (less than $20\,mN\,m^{-1}$) at the CMC, a large dynamic tension range can be investigated.

The cost is a factor of ten cheaper than the equivalent deuterated compound—an important consideration since sample volumes are around 2 litres.

7.1. *Surface tension*

Equilibrium tensions measured using DVT allow the dynamic effects due to impurities to be carefully monitored. EDTA was present in all the samples at a ratio

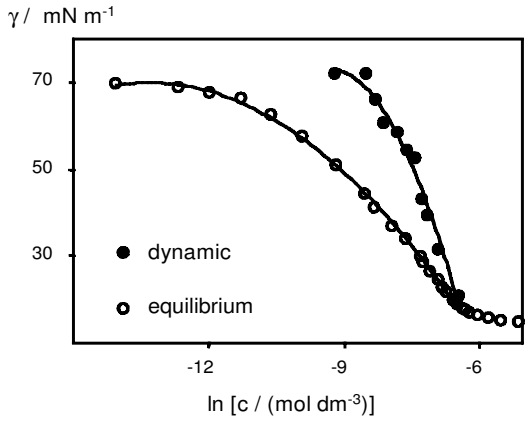

Figure 13. Surface tension of di-CF4 solutions at 30°C. Equilibrium tensions measured by the drop-volume method; dynamic measurements determined by SLS using the OFC.

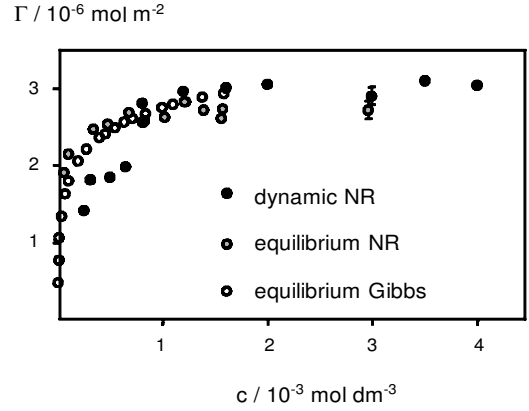

Figure 14. Adsorption isotherms for di-CF4 at 30°C. The curve (○) was obtained by applying equation (1) to the equilibrium tensiometric data of figure 13. Equation (35) was employed to analyse the neutron data which were measured using a standard trough (◎) or on the OFC (●).

of 1:25 to sequester divalent cation impurities [22, 38–42]. The $\gamma - \ln c$ plot is given in figure 13 and the CMC, 1.58 ± 0.3 mmol dm^{-3}, is clearly defined with no minimum or shoulder. As expected for a fluorocarbon the surface tension at the CMC is low, at (17.7 ± 0.1) mN m^{-1}.

The dynamic curve was measured using SLS on the OFC. At the CMC the surface tension is 20.6 ± 0.5 mN m^{-1}, close to the equilibrium value. However, as the concentration is decreased, the surface tension data quickly deviate from equilibrium, as the dynamic effect becomes significant.

7.2. *Neutron reflection*

Figure 14 shows adsorption isotherms for both equilibrium and dynamic behaviour on the OFC obtained by NR. The plot includes a curve inferred from

equilibrium surface tensions using equation (1), with $n = 2$ [22]. The agreement between the equilibrium isotherms is reasonably good. The dynamic adsorption agrees very well with the tensiometric data and remains in a plateau until CMC/2; at this point the adsorption decreases. Note that various repeat measurements and reproducibility checks have been made, and the error bars are representative of these findings.

It is noteworthy that, in comparing figures 13 and 14, $\Gamma(t)$ and Γ_{eq} are very similar, although the dynamic tensions are measurably higher than equilibrium values. Only small changes in Γ, within the error of NR, result in large changes in γ. Thus, Γ is largely insensitive to changes in surface tension at higher surface coverage, that is close to the CMC.

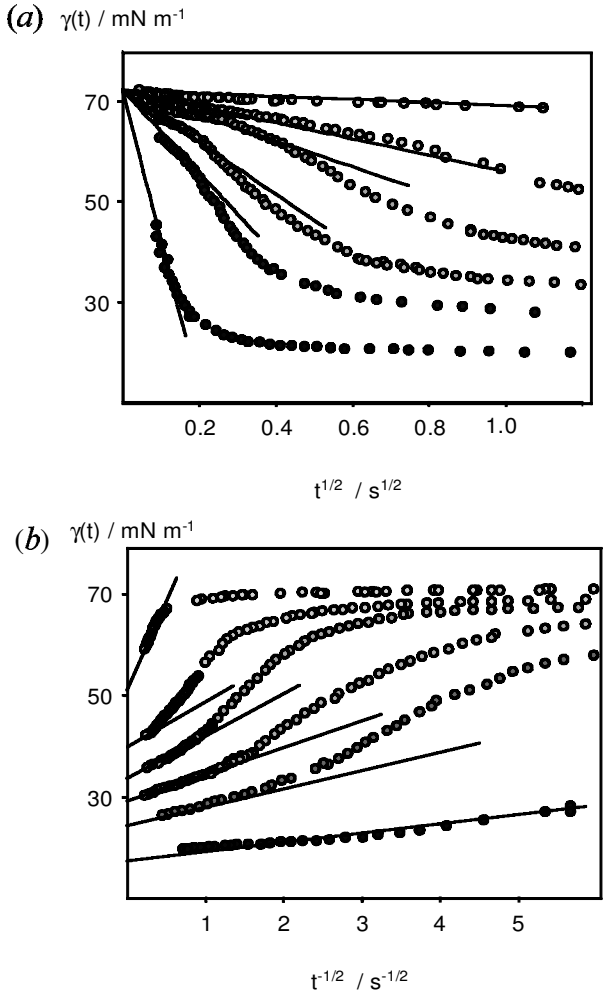

Figure 15. DSTs for di-CF4 solutions at 30°C determined by MBP tensiometry, where the concentrations are 0.1, 0.3, 0.5, 0.7, 1.0 and 1.58 mmol dm^{-3} showing (*a*) the limiting behaviour at a short time as given by equation (6) and (*b*) the long-time limit as described by equation (8): (——), least-squares fits using parameters as indicated in the text.

7.3. *Maximum-bubble-pressure experiments*

Measurements were also made with the MBP method and compared with the theoretical behaviour predicted by the diffusion-only model in equations (6) and (8). Figure 15 gives representative data with a few concentrations as examples. Figure 15 (*a*) shows the DST decay at short times with corresponding linear fits in line with equation (6). Similarly, figure 15 (*b*) shows the DST at long times and linear behaviour consistent with equation (8).

The equations of these lines were used to generate diffusion coefficients, as explained in section 4. Note that $\Gamma(t)$ values measured independently by NR, as shown in figure 14, have been used in calculating the expected gradients. For short times, in figure 15 (*b*), the calculated and fitted gradients agree well but, at long times equation (8) underestimates $\gamma(t)$. In order to achieve better agreement, the condition $D = D_{\text{monomer}}$ can be relaxed and an effective diffusion coefficient D_{eff} can be introduced, as before in section 4. Clearly $D_{\text{eff}} < D_{\text{monomer}}$ would be consistent with activated diffusion and this is the case here, where $D_{\text{eff}}/D_{\text{monomer}}$ varies between 0.02 (0.1 mmol dm^{-3}) and 1.35 (1.58 mmol dm^{-3}). These changes (described below in section 8 and figure 17) suggest a switch-over in adsorption mechanism from activated diffusion at low concentrations to essentially a diffusion-controlled mechanism at higher concentrations. This behaviour has been observed before using the OFC with NR, LDV and ellipsometry, for the cationic cetyltrimethylammonium bromide (CTAB), although a more detailed analysis was employed [7].

7.4. *Laser Doppler velocimetry*

The expansion rate of the OFC was measured by LDV and, as figure 16 shows, there is a marked concentration dependence, with a maximum in the expansion rate at about $\frac{2}{3}$ CMC. Rearranging equation (8) in terms of reciprocal time gives

$$\text{expansion rate}\,(\text{s}^{-1}) = \frac{[\gamma(t) - \gamma_0]^2 c^2 D}{\pi[RT\Gamma(t)^2]^2}. \tag{36}$$

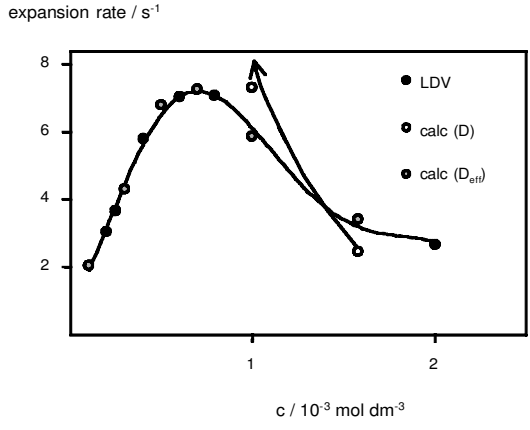

Figure 16. Measured surface expansion rate on the OFC as a function of di-CF4 concentration (●). The calculations are using equation (36) with the known monomer diffusion coefficient D (○) and using effective diffusion coefficients derived from the MBP measurements shown in figure 15 (◎).

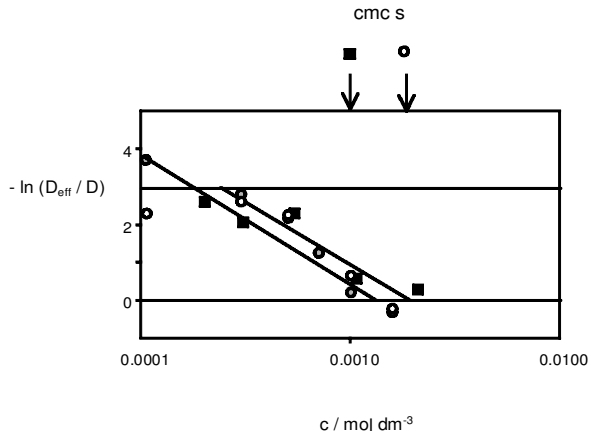

Figure 17. Diffusion coefficient ratio versus concentration for di-CF4 determined by MBP (○) and on the OFC (◉): (■), data are for the cationic surfactant *n*-hexylammonium dodecylsulphate determined by MBP (taken from [33]). Arrows indicate the respective CMCs. The lines of negative gradient are guides to the eye. The horizontal line at $-\ln(D_{\text{eff}}/D) \approx 3.0$ represents the mean value for all the non-ionic surfactants given in figure 8, and the limit $\ln(D_{\text{eff}}/D) = 0$ represents a purely diffusion controlled-mechanism.

Using equation (36), the expansion rate can be calculated from the MBP data, as all the other parameters are known. This is the second curve on figure 16, which clearly is inconsistent with the measured data points and in fact continues to increase exponentially with decreasing concentration. Once again, as for MBP, an effective diffusion coefficient can be introduced to achieve much better agreement. These calculated points are also shown, overlapping the original LDV data. In fact, as can be seen in figure 17 in the next section, the best-fit values of D_{eff} were almost identical with those found in the MBP experiments. This tends to suggest that the underlying mechanism is the same at the highly curved (MBP) and planar (OFC) interfaces, and that both methods are probing the same phenomena.

8. General behaviour for non-ionic and ionic surfactants

In figure 17 are compared results from 11 different surfactants that we have studied [33–37, 54, 60]. In this plot the purely diffusion-controlled limit is marked by a horizontal line at zero. For clarity an average value for D_{eff}/D of $0.05\,(\ln(0.05) \approx -3)$, shown by a line, has been taken from figure 8 for the nine non-ionics. Recall that there was no obvious effect of concentration on the effective diffusion coefficient for these compounds. The additional data points are for two charged surfactants, the di-CF4 (by MBP and OFC-LDV) and the catanionic surfactant *n*-hexylammonium dodecylsulphate (MBP), for which the structure is shown in figure 3(*e*). These latter data points are taken from [33].

Evidently the general behaviour of charged systems is different from that of the neutrals. In particular, there appears to be a switch-over in mechanism for both ionics as a function of concentration. At low concentrations the plot is consistent with a weak activated-diffusion adsorption, and the absolute ratios D_{eff}/D are similar to the non-ionics at equivalent concentrations. Surprisingly, and counter-intuitively, the tendency is toward diffusion control at high concentrations, and on

approaching the CMC. Around the CMC, for both ionics, the $\gamma(t)$ curves in the near-equilibrium limit can be adequately described by equation (8), with the monomer diffusion coefficients that have been inferred from independent NMR measurements. As discussed above, similar behaviour has been documented with a cationic surfactant CTAB [7], suggesting that this concentration-dependent mechanism may be a general phenomenon for charged surfactants.

Any theoretical basis for these differences in behaviour has not been dealt with adequately in the literature. Charge effects have been considered by MacLeod and Radke [97], who concluded that for anionic surfactants the rates of adsorption are approximately an order of magnitude lower than non-ionics under similar conditions. This can be thought of as arising because anionics have a larger adsorption barrier, although such differences are not displayed by our results in figure 17: quite the opposite! We find that with the ionics there is a strong concentration effect and, in contrast with the prediction, at high bulk concentrations, adsorption of ionics is essentially diffusion controlled, whereas non-ionics adsorb at a slower rate. Clearly, there is scope for theoretical input, to help to rationalize the observed behaviour.

9. Conclusions and outlook

DST and adsorption has been studied for a number of well-defined surfactants using a variety of methods, and there is now a large body of reliable data from different laboratories. Combined results from the MBP method, the drop-volume method, SLS and ellipsometric tensiometry, as well as surface excesses measured directly by NR and diffusion coefficients from NMR, allow clear conclusions to be drawn about the underlying adsorption mechanisms. In the limit of short times all the systems studied fit a diffusion-controlled model. However, at longer times, and especially for higher concentrations approaching and exceeding the CMC, significant deviations may be observed. For non-ionic surfactants, both temperature- and concentration-dependent studies are consistent with activated diffusion. With ionic surfactants, there is now compelling evidence to indicate a concentration-induced shift in mechanism: from activated diffusion at low concentrations, to diffusion only as the concentration is increased.

Fresh theoretical input is required to rationalize this behaviour to provide further insights into adsorption dynamics. This should facilitate experimental advances, allowing more complex and commercially relevant problems to be confidently tackled, for example DSTs of surfactant mixtures, surfactant–polymer mixtures and phospholipid–protein mixtures such as found in pulmonary surfactants.

Acknowledgements

We would like to thank Samantha Manning-Benson, Dmitrii Strykas and Gemma Shearman (from Oxford), Donal Sharpe, Simon Stebbing, Adrian Downer, Sandrine Nave and Alison Paul (from Bristol), Jeff Penfold and John Webster (ISIS, Rutherford Appleton Laboratory, UK) and Alan Pitt (Kodak UK) for stimulating discussions and experimental assistance. This project was funded by the Engineering and Physical Sciences Research Council (EPSRC) under grants GR/M83780, GR/M83797, GR/K85247 and GR/K04774. A.R. thanks EPSRC for a studentship. An allocation of neutron beam time and a grant were awarded by CCLRC (ISIS).

References

[1] Chang, C.-H., and Franses, E. I., 1995, *Colloid Surf.* A, **100,** 1.
[2] Miller, R., Fainerman, V. B., Schanko, K. H., Hofmann, A., and Heyer, W., 1997, *Tenside*, **34**, 357.
[3] Miller, R., Zholob, S. A., Makievski, A. V., Joos, P., and Fainerman, V. B., 1997, *Langmuir*, **13**, 5663.
[4] Hutchison, J., Klenerman, D., Manning-Benson, S., and Bain, C. D., 1999, *Langmuir*, **15**, 7530.
[5] Horozov, T., and Arnaudov, L., 1999, *J. Colloid Interface Sci.*, **219**, 99.
[6] Hsu, C. T., Shao, M. J., Lee, Y. C., and Lin, S. Y., 2000, *Langmuir*, **16**, 4846.
[7] Bain, C. D., Manning-Benson, S., and Darton, R. C., 2000, *J. Colloid Interface Sci.*, **229**, 247.
[8] Manning-Benson, S., Bain, C. D., Darton, R. C., Sharpe, D., Eastoe, J., and Reynolds, P., 1997, *Langmuir*, **13**, 5808.
[9] Manning-Benson, S., Parker, S. R. W., Bain, C. D., and Penfold. J., 1998, *Langmuir*, **14**, 990.
[10] Lu, J. R., Thomas, R. K., and Penfold, J., 2000, *Adv. Colloid Interface Sci.*, **84**, 143.
[11] Penfold. J., 2000, *Cur. Sci.,* **78**, 1458.
[12] Oh, S. G., Klein, S. P., and Shah, D. O., 1992, *AiChE Jl*, **38**, 149.
[13] Miller, R., 1997, *J. Colloid Interface Sci.*, **186**, 149.
[14] Danov, R. D. , 1996, *J. Colloid Interface Sci.*, **183**, 223.
[15] Lunkenheimer, K., Winsel, K., Furhner, J., Wantke, K. D., and Seigler, K., 1996, *Colloid Surf.* A, **114**, 199.
[16] Gibbs, J. W., 1906, *Papers of J. Willard Gibbs*, edited by H. A. Bumstead and R. G. van Name (London: Longmans Green), reprinted 1991 (New York: Dover Publications).
[17] Lu, J. R., Simister, E. A., Thomas, R. K., Lee, E. M., Rennie, A. R., and Penfold, J., 1992, *Langmuir*, **8**, 1837.
[18] Thomas, R. K., Lu, J. R., Lee, E. M., Penfold, J., and Flitsch, S. L., 1993, *Langmuir*, **9**, 1352.
[19] Eastoe, J., 1995, *New Physico-Chemical Techniques for the Characterisation of Complex Food Systems*, edited by E. Dickinson (London: Blackie), chapter 12.
[20] Hines, J. D., Garrett, P. R., Rennie, G. K., Thomas, R. K., and Penfold, J., 1997, *J. phys. Chem.* B, **101**, 7121.
[21] Hines, J. D., Garrett, P. R., Rennie, G. K., Thomas, R. K., and Penfold, J., 1997, *J. phys. Chem.* B, **101**, 9215.
[22] Eastoe, J., Nave, S., Downer, A., Paul, A., Rankin, A., Tribe, K., and Penfold, J., 2000, *Langmuir*, **16**, 4511.
[23] Hansen, R. S., 1960, *J. phys. Chem.*, **64**, 637.
[24] Hansen, R. S., 1961, *J. Colloid Sci.*, **16**, 585.
[25] Sutherland, K. L., 1952, *Aust. J. Sci. Res.* A, **5**, 683.
[26] Fainerman, V. B., Makievski, A. V., and Miller, R., 1994, *Colloid Surf.* A, **87**, 61.
[27] Baret, J. F., 1968, *J. phys. Chem.*, **72**, 2755.
[28] Ravera, F., Liggieri, L., and Steinchen, A., 1993, *J. Colloid Interface Sci.*, **156**, 109.
[29] Liggieri, L., Ravera, F., and Passerone, A., 1996, *Colloid Surf.* A, **114**, 351.
[30] Ravera, F, Liggieri, L., and Miller, R., 2000, *Colloid Surf.* A, **175**, 51.
[31] Liggieri, L., Ferrari, M., Massa, A., and Ravera, F., 2000, *Colloid Surf.* A, **175**, 51
[32] Ferrari, M., Liggieri, L., and Ravera, F., 1998, *J. phys. Chem.* B, **102**, 10521.
[33] Eastoe, J., Dalton, J. S., Rogueda, P. G. A., Sharpe, D., Dong, J., and Webster, J. R. P., 1996, *Langmuir*, **12**, 2706.
[34] Eastoe, J., Dalton, J. S., Rogueda, P. G. A., Crooks, E.R, Pitt, A. R., and Simister, E. A., 1997, *J. Colloid Interface Sci.*, **188**, 423.
[35] Eastoe, J., Dalton, J. S., Rogueda, P. G. A., and Griffiths, P. C., 1998, *Langmuir*, **14**, 979.
[36] Eastoe, J., Dalton, J. S., and Heenan, R. K., 1998, *Langmuir*, **14,** 5719.
[37] Dalton, J. S., 1998, PhD Thesis, University of Bristol.
[38] Downer, A., Eastoe, J., Pitt, A. R., Simister, E. A., and Penfold, J., 1999, *Langmuir*, **15,** 7591.

[39] Cross, A. W., and Jayson, G. G., 1994, *J. Colloid Interface Sci.*, **162**, 45.
[40] An, S. W., Lu, J. R., Thomas, R. K., and Penfold, J., 1996, *Langmuir*, **12**, 2446.
[41] Li, Z. X., Lu, J. R., and Thomas, R. K., 1997, *Langmuir*, **13**, 3681.
[42] Downer, A. D., Eastoe, J., Pitt, A. R., Penfold, J., and Heenan, R. K., 1999, *Colloid Surf.* A, **156**, 33.
[43] Lunkenheimer, K., Haage, K., and Hirte, R., 1999, *Langmuir*, **15**, 1052.
[44] Miller, R., Joos, P., and Fainerman, V. B., 1994, *Adv. Colloid Interface Sci.*, **49**, 249.
[45] Fainerman, V. B., 1985, *Russ. Chem. Rev.*, **54**, 948.
[46] Padday, J. F., 1969, *Surface and Colloid Science*, Vol. 1, edited by E. Matijevic (New York: Wiley–Interscience).
[47] Harkins, W., and Brown, F. E., 1991, *J. Am. chem. Soc.*, **41**, 499.
[48] Tornberg, E., 1978, *J. Colloid Interface Sci.*, **64**, 435.
[49] Dukhin, S. S., Kretzschmar, G., and Miller, R., 1995, *Dynamics of Adsorption at Liquid Interfaces* (Amsterdam: Elsevier).
[50] Fainerman, V. B., and Miller, R., 1995, *J. Colloid Interface Sci.*, **175**, 118.
[51] Lylyk, S. V., Makievski, A. V., Koval'chuck, V. I., Schano, K. H., Fainerman, V. B., and Miller, R., 1998, *Colloid Surf.* A, **135**, 27
[52] Lin, S.-Y., Tsay, R.-Y., Lin, L.-W., and Chen, S.-I., 1996, *Langmuir*, **12**, 6530.
[53] Chang, H.-C., Hsu, C.-T., and Lin, S.-I., 1998, *Langmuir*, **14**, 2476.
[54] Eastoe, J., and Dalton, J. S., 2000, *Adv. Colloid Interface Sci.*, **85**, 103.
[55] Lin, S.-Y., Tsay, R.-Y., Lin, L.-W., and Chen, S.-I., 1996, *Langmuir*, **12**, 6530.
[56] Lin, S-Y., McKeigue, K., and Maldarelli, C., 1991, *Langmuir*, **7**, 1055.
[57] Eastoe, J., Rogueda, P., Harrison, W. J., Howe, A. M., and Pitt, A. R., 1994, *Langmuir*, **10**, 4429.
[58] Eastoe, J., Rogeuda, P., Howe, A. M., Pitt, A. R., and Heenan, R. K., 1996, *Langmuir*, **12**, 2701.
[59] Cooke, D. J., Lu, J. R., Lee, E. M., Thomas, R. K., Pitt, A. R., and Simister, E. A., 1996, *J. phys. Chem*, **100**, 10298.
[60] Rogueda, P. G. A., 1996, PhD Thesis, University of Bristol.
[61] Griffiths, P. C., Stilbs, P., Paulson, K., Howe, A. M., and Pitt, A. R., 1997, *J. phys. Chem*, **101**, 915.
[62] Makievski, A. V., Fainerman, V. B. , Miller, R., Bree, M., Liggieri, L., and Ravera, F., 1997, *Colloid Surf.* A, **122**, 269.
[63] Filippov, L. K., 1994, *J. Colloid Interface Sci.*, **163**, 49.
[64] Filippov, L. K., 1994, *J. Colloid Interface Sci.*, **164**, 471.
[65] Filippov, L. K., 1996, *J. Colloid Interface Sci.*, **182**, 330.
[66] Filippov, L.K , and Filippova, N. L., 1996, *J. Colloid Interface Sci.*, **178**, 571.
[67] Svitova, T., Hoffmann, H., and Hill, R. M., 1996, *Langmuir*, **12**, 1712.
[68] Rosen, M. J., and Song, L. D., 1996, *J. Colloid Interface Sci.*, **179**, 261.
[69] Aniannson, E. A. G., and Wall, S. N., 1974, *J. phys. Chem.*, **78**, 1024.
[70] Aniannson, E. A. G., and Wall, S. N., 1975, *J. phys. Chem.*, **79**, 857.
[71] Aniannson, E. A. G., *et al.* 1976, *J. phys. Chem.*, **80** 905.
[72] Rillaerts, E., and Joos, P., 1982, *J. phys. Chem.*, **86,** 3471.
[73] Fainerman, V. B., 1992, *Colloid Surf.*, **62,** 333.
[74] Fainerman, V. B., and Makievski, A. V., 1992, *Kolloid Z. (Engl. Edn)*, **54**, 890.
[75] Fainerman, V. B., and Makievski, A. V., 1992, *Kolloid Z. (Engl. Edn)*, **54**, 897.
[76] Fainerman, V. B., and Makievski, A. V. 1993, *Colloid Surf.*, **69,** 249.
[77] Tiberg, F., Jonsson, B., and Lindman, B., 1994, *Langmuir*, **10**, 3714.
[78] Johner, A., and Joanny, J. F., 1990, *Macromolecules*, **23**, 5299.
[79] Padday, J. F., 1957, *Proceedings of the International Congress on Surface Actuation*, p. 1.
[80] Bergink-Martens, D. J. M., Bos, H. J., Prins, A., and Schulte, B. C., 1990, *J. Colloid Interface Sci.*, **138**, 1.
[81] Bergink-Martens, D. J. M., Bos, H. J., and Prins, A., 1994, *J. Colloid Interface Sci.*, **165,** 221.
[82] DeFeijter, J. A., Benjamin, J., and Veer, F. A., 1978, *Biopolymers*, **17**, 1759.
[83] Drain, L. E, 1980, *The Laser Doppler Technique* (Chichester, West Sussex: Wiley).

[84] DURST, F., MELLING, A., and WHITELAW, H. J., 1981, *Principles and Practice of Laser-Doppler Anemometery*, second edition (London: Academic Press).
[85] EARNSHAW, J. C., 1999, *J. Dispersion Sci. Technol.*, **20**, 743.
[86] EARNSHAW, J. C., MCGIVERN, R. C., MCLAUGHLIN, A. C., and WINCH, P. J., 1990, *Langmuir*, **6**, 649.
[87] SHARPE, D. J., 1995, PhD Thesis, Queen's University, Belfast.
[88] SHARPE, D. J., and EASTOE, J., 1996, *Langmuir*, **12**, 2303.
[89] TAJIMA, K., MURAMATSU, M., and SASAKI, T., 1970, *Bull. chem. Soc. Japan*, **43,** 1991.
[90] TAJIMA, K., 1970, *Bull. chem. Soc. Japan*, **43**, 3063.
[91] TAJIMA, K., 1971, *Bull. chem. Soc. Japan*, **44**, 1767.
[92] BAE, S., HAAGE, K., WANTKE, K., and MOTSCHMANN, H., 1999, *J. phys. Chem.* B, **103**, 1045.
[93] LI, Z. X., DONG, C. C., and THOMAS, R. K., 1999, *Langmuir*, **15**, 4392.
[94] SIMISTER, E. A., THOMAS, R. K., PENFOLD, J., AVEYARD, R., BINKS, B. P., COOPER, P., FLETCHER, P. D. I., LU, J. R., and SOKOLOWSKI, A., 1992, *J. phys. Chem*, **96**, 1383.
[95] http://www.isis.rl.ac.uk/
[96] PENFOLD, J., and THOMAS, R. K., 1990, *J. Phys.: condens. Matter*, **2**, 1369.
[97] MACLEOD, C. A., and RADKE, C. J., 1993, *J. Colloid Interface Sci.*, **160**, 435.